The role of propagating modes in silver nanowire arrays for transparent electrodes

Tongchuan Gao and Paul W. Leu*

Department of Industrial Engineering, University of Pittsburgh, Pittsburgh, PA 15261, USA

**pleu@pitt.edu*

http://lamp.pitt.edu

Abstract: Silver nanowires have been shown to demonstrate enhanced transmission and promising potential for next-generation transparent electrodes. In this paper, we systematically investigated the electrical and optical properties of 1D and 2D silver nanowire arrays as a function of diameter and pitch and compared their performance to that of silver thin films. Silver nanowires were found to exhibit enhanced transmission over thin films due to propagating resonance modes between nanowires. We evaluated the angular dependence and dispersion relation of these propagating modes and demonstrate that larger nanowire diameters and pitches are favored for achieving higher solar transmission at a particular sheet resistance. Silver nanowires may achieve achieve solar transmission $> 90\%$ with sheet resistances of a few Ω/sq and figure of merit $\sigma_{dc}/\sigma_{op} > 1000$.

OCIS codes: (350.6050) Solar energy; (310.6628) Subwavelength structures; (160.2100) Electro-optical materials; nanostructures.

References and links

1. C. G. Granqvist and A. Hultåker, "Transparent and conducting ITO films: new developments and applications," Thin Solid Films **411**, 1–5 (2002).
2. A. Kumar and C. Zhou,"The race to replace tin-doped indium oxide: which material will win? ," ACS Nano **4**, 11–14 (2010).
3. A. C. Tolcin, "Indium," USGS Mineral Commodity Summary (2011).
4. T. Minami, "Present status of transparent conducting oxide thin-film development for Indium-Tin-Oxide (ITO) substitutes," Thin Solid Films **516**, 5822–5828 (2008).
5. Z. Chen, B. Cotterell, W. Wang, E. Guenther, and S. Chua, "A mechanical assessment of flexible optoelectronic devices," Thin Solid Films **394**, 201–205 (2001).
6. A. R. Madaria, A. Kumar, F. N. Ishikawa, and C. Zhou, "Uniform, highly conductive, and patterned transparent films of a percolating silver nanowire network on rigid and flexible substrates using a dry transfer technique," Nano Research **3**, 564–573 (2010).
7. X. Wang, L. Zhi, and K. Mullen, "Transparent, conductive graphene electrodes for dye-sensitized solar cells," Nano Lett. **8**, 323–327 (2008).
8. S. De, P. J. King, M. Lotya, A. O'Neill, E. M. Doherty, Y. Hernandez, G. S. Duesberg, and J. N. Coleman, "Flexible, transparent, conducting films of randomly stacked graphene from surfactant-stabilized, oxide-free graphene dispersions," Small **6**, 458–464 (2010).
9. M. W. Rowell, M. A. Topinka, M. D. McGehee, H. Prall, G. Dennler, N. S. Sariciftci, L. Hu, and G. Gruner, "Organic solar cells with carbon nanotube network electrodes," Appl. Phys. Lett. **88**, 233506 (2006).
10. C. F. Zhang, Z. W. Dong, G. J. You, S. X. Qian, and H. Deng, "Multiphoton route to ZnO nanowire lasers," Opt. Lett. **31**, 3345–3347 (2006).

#183390 - $15.00 USD Received 14 Jan 2013; revised 3 Apr 2013; accepted 4 Apr 2013; published 17 Apr 2013

11. Y. Zhou, L. Hu, and G. Grüner, "A method of printing carbon nanotube thin films," Appl. Phys. Lett. **88**, 123109 (2006).
12. S. De, T. M. Higgins, P. E. Lyons, E. M. Doherty, P. N. Nirmalraj, W. J. Blau, J. J. Boland, and J. N. Coleman, "Silver nanowire networks as flexible, transparent, conducting films: Extremely high DC to optical conductivity ratios," ACS Nano **3**, 1767–1774 (2009).
13. L. Hu, H. S. Kim, J. Lee, P. Peumans, and Y. Cui, "Scalable coating and properties of transparent, flexible, silver nanowire electrodes," ACS Nano **4**, 2955–2963 (2010).
14. P. E. Lyons, S. De, J. Elias, M. Schamel, L. Philippe, A. T. Bellew, J. J. Boland, and J. N. Coleman, "High-Performance transparent conductors from networks of gold nanowires," J. Phys. Chem. Lett. **2**, 3058–3062 (2011).
15. J. Lee, S. T. Connor, Y. Cui, and P. Peumans, "Solution-processed metal nanowire mesh transparent electrodes," Nano Lett. **8**, 689–692 (2008).
16. Y. C. Lu and K. S. Chou, "Tailoring of silver wires and their performance as transparent conductive coatings," Nanotechnology **21**, 215707 (2010).
17. S. Sorel, P. E. Lyons, S. De, J. C. Dickerson, and J. N. Coleman, "The dependence of the optoelectrical properties of silver nanowire networks on nanowire length and diameter," Nanotechnology **23**, 185201 (2012).
18. S. M. Bergin, Y. Chen, A. R. Rathmell, P. Charbonneau, Z. Li, and B. J. Wiley, "The effect of nanowire length and diameter on the properties of transparent, conducting nanowire films," Nanoscale **4**, 1996 (2012).
19. S. De, P. J. King, P. E. Lyons, U. Khan, and J. N. Coleman, "Size effects and the problem with percolation in nanostructured transparent conductors," ACS Nano **4**, 7064–7072 (2010).
20. J. van de Groep, P. Spinelli, and A. Polman, "Transparent conducting silver nanowire networks," Nano Letters, **12** 3138–3144 (2012).
21. P. B. Catrysse and S. Fan, "Nanopatterned metallic films for use as transparent conductive electrodes in optoelectronic devices," Nano Lett. **10**, 2944–2949 (2010).
22. P. B. Catrysse and S. Fan "Propagating plasmonic mode in nanoscale apertures and its implications for extraordinary transmission," J. Nanophoton. **2** (1), 021790 (2008).
23. J. A. Porto, F. J. García-Vidal, and J. B. Pendry, "Transmission resonances on metallic gratings with very narrow slits," Phys. Rev. Lett. **83**, 2845 (1999).
24. K. Yee, "Numerical solution of initial boundary value problems involving maxwell's equations in isotropic media," Antennas and Propagation, IEEE Transactions on **14**, 302–307 (1966).
25. A. Taflove, "Application of the finite-difference time-domain method to sinusoidal steady-state electromagnetic-penetration problems," Electromagnetic Compatibility, IEEE Transactions on **EMC-22**, 191–202 (1980).
26. E. D. Palik and G. Ghosh, *Handbook of Optical Constants of Solids* (Academic Press, 1998).
27. J. Berenger, "A perfectly matched layer for the absorption of electromagnetic waves," J. Comput. Phys. **114**, 185–200 (1994).
28. "Solar spectral irradiance: Air mass 1.5".
29. B. R. Cooper, H. Ehrenreich, and H. R. Philipp, "Optical properties of noble metals. II.," Phys. Rev. **138**, A494–A507 (1965).
30. D. Lide, *CRC Handbook of Chemistry and Physics* (CRC press, 2012).
31. A. J. McAlister and E. A. Stern, "Plasma resonance absorption in thin metal films," Phys. Rev. **132**, 1599–1602 (1963).
32. E. Popov, M. Nevière, S. Enoch, and R. Reinisch, "Theory of light transmission through subwavelength periodic hole arrays," Phys. Rev. B **62**, 16100–16108 (2000).
33. Y. Takakura, "Optical resonance in a narrow slit in a thick metallic screen," Phys. Rev. Lett. **86**, 5601–5603 (2001).
34. U. Fano, "Effects of configuration interaction on intensities and phase shifts," Phys. Rev. **124**, 1866–1878 (1961).
35. M. W. Rowell and M. D. McGehee, "Transparent electrode requirements for thin film solar cell modules," Energy Environ. Sci. **4**, 131–134 (2011).
36. M. Dressel and G. Grüner, *Electrodynamics of Solids: Optical Properties of Electrons in Matter* (Cambridge University Press, 2002).
37. P. N. Nirmalraj, P. E. Lyons, S. De, J. N. Coleman, and J. J. Boland, "Electrical connectivity in single-walled carbon nanotube networks," Nano Lett. **9**, 3890–3895 (2009).

1. Introduction

Transparent conductors are important as the top electrode for a variety of optoelectronic devices, such as solar cells, flat panel displays, touch screens, and light-emitting diodes. Currently, the most common transparent electrode is indium tin oxide ($In_{2-x}Sn_xO_3$:ITO) films [1] which have a combination of high optical transparency (> 80 %) and low resistivity ($\approx 10^{-6}$ Ω·m) [2]. However, ITO suffers from several economic and technological short comings: (1) indium is

#183390 - $15.00 USD Received 14 Jan 2013; revised 3 Apr 2013; accepted 4 Apr 2013; published 17 Apr 2013

a scarce resource subject to increasing price [3], (2) ITO deposition methods are costly [4], (3) ITO is a brittle material, preventing its use in emerging flexible devices [5], and (4) ITO requires high processing temperatures making it unsuitable for organic devices [6]. Fundamentally, transparent conductor films suffer from a tradeoff between sheet resistance and optical transmission. These films must be made thicker or doped more heavily in order to decrease sheet resistance, but this decreases optical transmission.

Recently, several new materials, such as graphene [7, 8], random carbon nanotube films [9–11], and random metal nanowire films [12–14] have emerged as promising next-generation transparent conductors that may be assembled through scalable processes and for flexible optoelectronics [15]. Amongst these new materials, random metal nanowire films appear to be the most promising due to their combination of high sheet conductivity and high optical transmission [12–14]. There have been some systematic studies on the dependence of the optical and electrical properties of random metal nanowire films on geometry [16–18], though these random films tend to be limited by connectivity when sparse [19]. Two dimensional silver nanogratings have been fabricated and a variety of wire widths, heights, and pitches have been studied [20]. Subwavelength metal gratings have also been studied theoretically for transparent electrodes [21], but this study only investigated gratings with pitch $a = 600$ nm. There have yet to be any systematic and detailed theoretical studies on circular cross-section nanowires for transparent electrodes.

In this paper, we report on simulation studies of the optical and electrical properties of 1D and 2D silver nanowire arrays of circular cross-section with diameters from 5 to 400 nm and pitches from 5 to 2000 nm. We compare these results to that of silver thin films and demonstrate the role of propagating modes and surface plasmons in the enhanced transmission of silver nanowire arrays. Propagating modes or waveguide modes in the areas between the metal have been previously studied in cylindrical holes [22] and metallic gratings [23]. The angular dependence and dispersion relation of these propagating modes are discussed. The electrical and optical performance of various structures are compared and general design principles are elucidated. While silver thin films may achieve $T_{solar} = 90\%$ with sheet resistance 8 Ω/sq and figure of merit σ_{dc}/σ_{op} of about 440, silver nanowire arrays may achieve $T_{solar} > 90\%$ at sheet resistances of a few Ω/sq and $\sigma_{dc}/\sigma_{op} > 1000$.

2. Method

Figure 1 shows the schematic of the different transparent conductor systems we studied: (a) silver thin films defined by thickness t, (b) 1D silver nanowire arrays with diameter d and pitch a, and (c) 2D silver nanowire arrays. The 2D silver nanowire arrays are also defined by diameter d and the pitch a of the square lattice. Silver thin films thicknesses t = 1 to 158 nm were studied, and silver nanowire arrays with nanowire diameter range from d = 5 to 400 nm and pitches a from 5 to 2000 nm with $d \leq a$ were investigated. The optical properties were determined by solving Maxwell's questions using the finite difference time domain (FDTD) method [24, 25]. The optical constants for silver were taken from experimental measurement results in Palik's *Handbook of Optical Constants of Solids* [26]. A non-uniform simulation mesh with a finer mesh near interfaces and larger mesh in bulk regions was utilized. Perfectly matched layer boundary conditions were used for the upper and lower boundary of the simulation cell [27], while appropriate periodic boundary conditions were used for the side boundaries to model the periodic nature of the arrays. To study the performance of these different structures as transparent conductors, the solar integrated transmission was calculated from

$$T_{solar} = \frac{\int b(\lambda)T(\lambda)d\lambda}{\int b(\lambda)d\lambda} \tag{1}$$

#183390 - $15.00 USD Received 14 Jan 2013; revised 3 Apr 2013; accepted 4 Apr 2013; published 17 Apr 2013

where λ is the free-space wavelength, $b(\lambda)$ is the photon flux density, and $T(\lambda)$ is the optical transmission for light with wavelength λ. We considered the wavelength range λ = 280 to 1000 nm of the global 37° tilt AM1.5 solar spectrum [28].

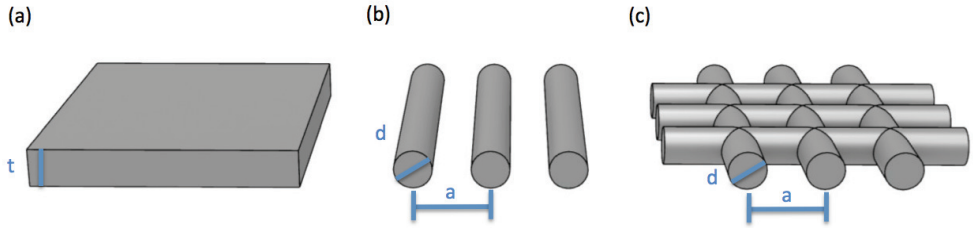

Fig. 1. Schematic of structures studied: (a) silver thin film with thickness t, (b) 1D silver nanowire array with pitch a and the diameter d, and (c) 2D silver nanowire array.

3. Results and Discussion

Figure 2(a) illustrates a contour plot of $T(\lambda)$ for silver thin films of thickness t. At larger wavelengths, photons are governed by free electron-like behavior as governed by the Drude model. Almost all of the incident light is reflected since the real part of the index of refraction is small and $R(\lambda) = |(n(\lambda)-1)/(n(\lambda)+1)|^2$ where $n(\lambda)$ is the complex index of refraction of silver and the index of refraction of air is 1. Below 310 nm, interband transitions from d electrons to the Fermi surface start to become important. The absorption edge is at about 320 nm (3.9 eV), which is associated with interband transitions from the L_{32} to $L_{2'}$ band [29]. Silver thin films have some reflection and high absorption for photons with lower wavelength than this absorption edge. The plasma frequency of the free electrons in the silver is about 130 nm (9.2 eV) and thus, photons across the entire solar spectrum range cannot propagate in silver. Silver films only support evanescent modes, where the electromagnetic field intensity decays exponentially from the front surface. The transmission in films is described by the skin depth, where transmission is possible when t is comparable or smaller than the skin depth. The skin depth of silver is slightly over 20 nm for most of the spectral range of interest and has a maximum at the 320 nm wavelength. Figure 2(b) plots T_{solar} with the same y-axis as in (a) with R_s shown on the right y-axis. $R_s = \rho_{bulk}/t$ where $\rho_{bulk} = 1.59 \times 10^{-8}$ Ω·m, which is the bulk silver resistivity [30]. Because the transmission is evanescent in silver thin films, T_{solar} rapidly decreases with increasing thickness. T_{solar} = 90% at $t = 2$ nm where $R_s = 8$ Ω/sq.

#183390 - $15.00 USD Received 14 Jan 2013; revised 3 Apr 2013; accepted 4 Apr 2013; published 17 Apr 2013

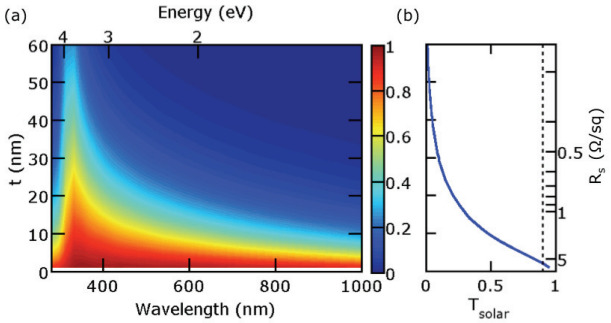

Fig. 2. (a) Transmission of different silver thin film thicknesses t for wavelengths $\lambda = 280$ to 1000 nm. (b) T_{solar} across the wavelengths shown for different thicknesses with the sheet resistance R_s labelled on the right y-axis. The y-axis in (b) is the same as in (a).

In order to compare the transmission properties of 1D ordered nanowire arrays with thin films, we evaluated the transmission characteristics of TE-polarized and TM-polarized incident light. The electric field is parallel to the axes of the nanowires for TE-polarized incident light and perpendicular for TM. Figure 3(a) plots $T(\lambda)$ as a function of diameter with $a = 600$ nm for TE-polarized incident light. The transmission has a small peak at 326 nm for the same reasons as the silver thin film discussed above. The transmission exhibits evanescent behavior except when propagating modes are supported between the silver nanowires. Due to the translational symmetry of the nanowire array as well as the mirror symmetry, these propagating modes occur when $k_0 \pm k_0 \sin\theta = 2\pi m/a$, where k_0 is the free space wave-vector, m is the mode number and a positive integer, and θ is the incident angle. Equivalently, this can be expressed as

$$\lambda = a(1 \pm \sin\theta)/m. \tag{2}$$

For normal-incident light (θ = 0), the propagating modes exist at $\lambda = a/m$. Due to these propagating resonant TE modes, nanowire arrays have higher T_{solar} for TE-incident light compared to thin films at the same R_s as shown in Fig. 3(b). $R_s = 4\rho_{bulk}a/\pi d^2$ for 1D silver nanowire arrays. T_{solar} = 90% at $d = 90$ nm and $a = 600$ nm where $R_s = 1.5$ Ω/sq. Figure 3(c) shows the electromagnetic field of the doubly-degenerate TE_1 and TE_2 modes under normal incidence in these Ag nanowire arrays. At these wavelengths, there is an enhanced electromagnetic field surrounding the nanowires leading to high transmission. These propagating modes begin to be cut off when $d > \lambda/2$ as the electromagnetic wave is unable to concentrate completely in the space around the nanowires.

#183390 - $15.00 USD Received 14 Jan 2013; revised 3 Apr 2013; accepted 4 Apr 2013; published 17 Apr 2013

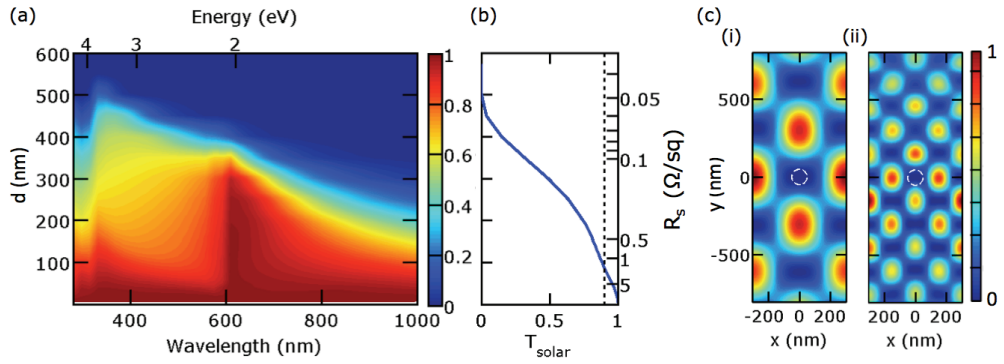

Fig. 3. Transmission characteristics of silver nanowire arrays for TE-incident light for $a =$ 600 nm. (a) Contour plot of T as a function of wavelength and nanowire diameter d. (b) T_{solar} over the wavelength range shown with the sheet resistance R_s shown in the right y-axis. (c) Electric field intensity $|E|^2$ for (i) TE_1 mode at $\lambda = 600$ nm and (ii) TE_2 mode at $\lambda = 300$ nm with $d = 80$ nm where the edge of the nanowire is shown with a dashed white line.

Figure 4(a) shows the angular dependence of propagating TE modes for 1D silver nanowire arrays with $a = 600$ nm and $d = 80$ nm. $R_s = 1.9\ \Omega$/sq. These modes are labelled with subscripts based on the mode number and $\pm$ in Eq. (2). The propagating modes are singly degenerate, except at the center of each Brillouin zone where $k_x = m2\pi/a$ and at the edges of the Brillouin zone where $k_x = (m+1/2)2\pi/a$. High transmission occurs at the propagating modes for TE-incident light. Other than these propagating modes, the electric field is evanescent at higher angles and thus T_{solar} decreases at higher angles as shown in Fig. 4(b). $T_{solar} = 91\%$ at normal incidence and drops below 90% at an incidence angle of 7°.

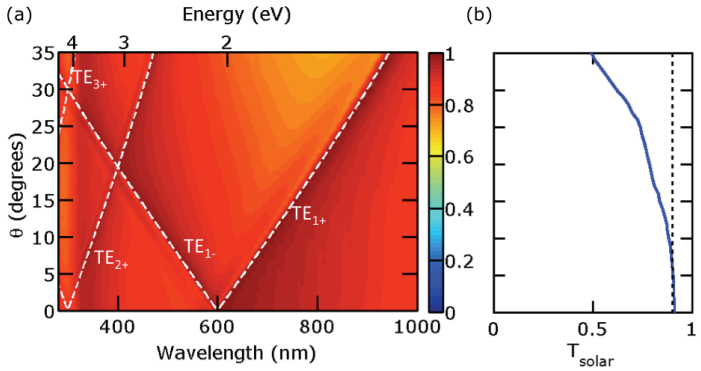

Fig. 4. Angular-dependence of silver nanowire arrays transmission for TE-incident light for $a = 600$ nm and $d = 100$ nm. (a) Contour plot of T as a function of wavelength and incident angle θ. (b) T_{solar} over the wavelength range with the same y-axis as in (a).

The TM transmission spectrum is shown in Fig. 5(a). Near $\lambda = 340$ nm for all nanowire arrays, there is a dip in the transmission spectrum due to enhanced absorption. This absorption is mostly independent of the silver nanowire diameter and due to the excitation of the surface plasmon of the silver, which can also be excited in thin films under non-normal TM incidence [31]. The dispersion relation of the TM modes are the same as those of the TE modes with one important difference–the existence of a TM_0 mode. The TE_0 mode does not exist because E_z

#183390 - $15.00 USD Received 14 Jan 2013; revised 3 Apr 2013; accepted 4 Apr 2013; published 17 Apr 2013

= 0 everywhere in order to satisfy the boundary conditions of $E_z = 0$ at the nanowire surface. In contrast, there exists a TM_0 mode which does not have a cutoff wavelength. This mode is, strictly speaking, a TEM mode since both the electric and magnetic field are transverse. It is a direct transmission process where the incident energy goes straight through the nanowires. This propagating mode is responsible for enhanced transmission in metallic nanoslits, regardless of how small these nano slits are [23,32,33]. From our contour plot, it was also noted that when the TM_0 mode is the only mechanism for enhanced transmission, the transmission resonance peak is approximately where the nanowire diameter is about half of the wavelength. Under these conditions, the magnetic field can concentrate in the space between the nanowires allowing for high transmission.

There are thus, two mechanisms for enhanced transmission in silver nanowire arrays under TM-incident light: direct transmission from a TM_0 mode and indirect propagating $TM_{m\pm}$ modes. T_{solar} is plot for the different diameter nanowire arrays shown in Fig. 5(b) and tends to be higher than that for TE-incident light due to the TM_0 mode. T_{solar} = 90% at $d = 120$ nm and $a = 600$ nm where $R_s = 0.8\ \Omega$/sq. The indirect TM propagating modes occur simultaneously with surface plasmon polariton (SPP) modes. Due to the periodic structure of the nanowires, surface plasmon polaritons can couple to incident light when $k_{SPP} = k_0 \sin\theta \pm m\frac{2\pi}{a}$, where m is a positive integer. The real part of the H_z field patterns at $\lambda = 589$ nm and 300 nm are shown in Fig. 5(c) and (d) respectively for (i) 50 and (ii) 200 nm diameter nanowires. For small diameter nanowires such as the 50 nm illustrated, the transmission is primarily due to direct transmission through the TM_0 mode. For larger diameter nanowires, the incident light couples more strongly to the indirect propagating modes. Due to interference between the two mechanisms for transmission at larger wavelengths, the transmission behavior exhibits Fano-type resonances with characteristic asymmetric peaks preceded by sharp dips [34]. For 200 nm diameter Ag nanowires, the dip in the transmission spectra at 589 nm and 300 nm result from interference between the TM_0 mode and TM_1 mode (Fig. 5cii) and the TM_2 mode (Fig. 5dii) respectively.

#183390 - $15.00 USD Received 14 Jan 2013; revised 3 Apr 2013; accepted 4 Apr 2013; published 17 Apr 2013

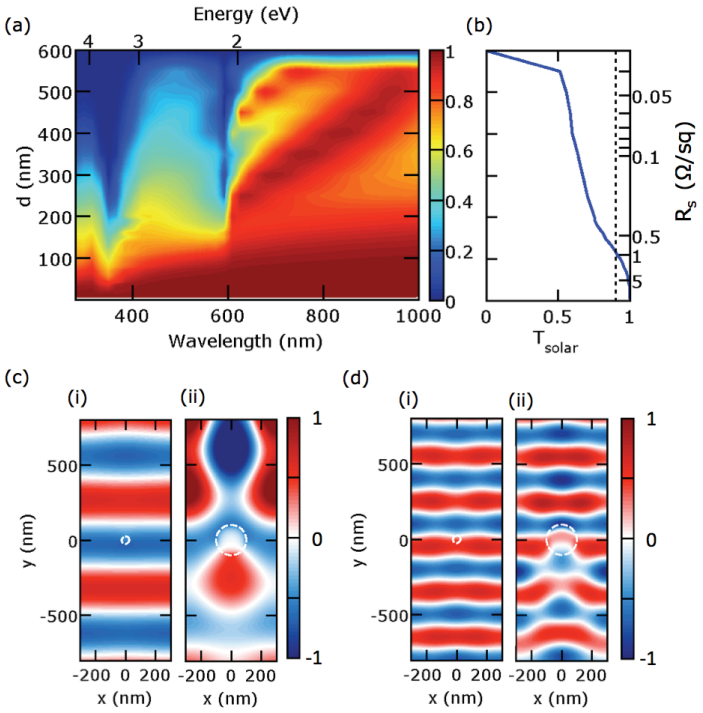

Fig. 5. Transmission characteristics of silver nanowire arrays for TM-incident light for $a = 600$ nm. (a) Contour plot of T as a function of wavelength and nanowire diameter d. (b) T_{solar} over the wavelength range shown with the same y-axis as in (a) and the sheet resistance R_s shown in the right y-axis. (c) Real part of H_z at $\lambda = 589$ nm for (i) 50 and (ii) 200 nm diameter silver nanowires. (d) Re(H_z) at $\lambda = 300$ nm for (i) 50 and (ii) 200 nm diameter silver nanowires.

In Fig. 6, we plot the angular dependence of the transmission of 1D silver nanowire arrays with $a = 600$ nm and $d = 80$ nm under different incidence angles for TM-polarized light. The transmission is high across the spectrum due to the TM_0 transmission pathway. The distinct dip in transmission near $\lambda = 340$ nm is due to the excitation of surface plasmons and independent of incidence angle. Enhanced absorption is associated with the surface plasmon. The dispersion relation of the TM modes, where the modes are again labelled with subscripts based on Eq. (2), is identical to that of the TE modes. For low incident angles the transmission is high across the spectrum as transmission is primarily due to the TM_0 mode for this small diameter nanowire array, but at higher angles the indirect transmission pathways become more important such that Fano resonances start to become evident. $T_{solar} = 96\%$ at normal incidence and drops below 90% at an incidence angle of 30° for TM-incident light.

#183390 - $15.00 USD Received 14 Jan 2013; revised 3 Apr 2013; accepted 4 Apr 2013; published 17 Apr 2013

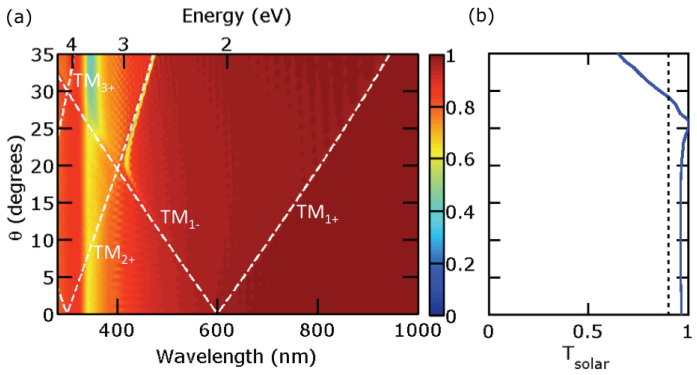

Fig. 6. Angular-dependence of Ag nanowire arrays transmission for TM-incident light for $a = 600$ nm and $d = 100$ nm. (a) Contour plot of T as a function of wavelength and incident angle θ. (b) T_{solar} over the wavelength range with the same y-axis as in (a).

Figure 7(a) shows T_{solar}, averaged for tranverse-electric (TE) and transverse-magnetic (TM) polarization for different 1D nanowire array sheet resistances R_s. $T_{solar} = 90\%$ and $R_s = 10$ Ω/sq are shown with dashed black lines, since both $T_{solar} \geq 90\%$ and $R_s \leq 10$ Ω/sq are important for transparent conductors in thin film solar cells [35]. Different diameter nanowires are represented by different color markers, and the pitch is indicated by the size of the marker. The curves show clear trends for solar transmission as a function of diameter d and pitch a. For the same R_s, nanowire arrays with larger diameter at the appropriate pitch have higher T_{solar}. This is because R_s decreases with $1/d^2$ while transmission decreases approximately proportional to d. It can also be seen from this figure that nanowire arrays are superior to thin films as they can achiever higher T_{solar} for the same R_s.

To further compare the performance of different silver nanowire array geometries for transparent electrodes, we plot in Fig. 7(b) the commonly used figure of merit for transparent electrodes σ_{dc}/σ_{op} [36] as a function of R_s where σ_{dc} is the DC conductivity of the material and σ_{op} is the optical conductivity. Higher values for this figures of merit indicate better performance. This figure of merit arises from $T_{solar} = \left(1 + \frac{Z_0}{2R_s}\frac{\sigma_{\mathrm{op}}}{\sigma_{\mathrm{dc}}}\right)^{-2}$, where $Z_0 = 377$ Ω is the free space impedance. This plot of figure of merit further demonstrates the improved performance of silver nanowire arrays over silver thin films as well as the improved performance of larger diameter nanowires over smaller diameter nanowires. In addition, these figures of merit allow for comparison between a wide range of materials and demonstrate that ordered silver nanowire arrays have the potential to exceed what has been currently fabricated experimentally. Random films of silver nanowires have exhibited $\sigma_{\mathrm{dc}}/\sigma_{\mathrm{op}}$ of about 500 [12] compared to about 0.5 for graphene thin films [7] and about 30 for random carbon nanotube meshes [37]. Our simulations indicate $\sigma_{\mathrm{dc}}/\sigma_{\mathrm{op}} > 1000$ may be achievable in ordered silver nanowire arrays.

#183390 - $15.00 USD Received 14 Jan 2013; revised 3 Apr 2013; accepted 4 Apr 2013; published 17 Apr 2013

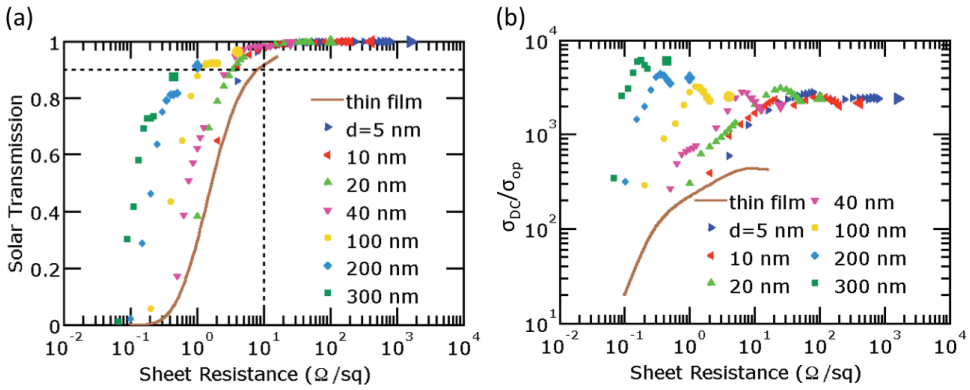

Fig. 7. (a) T_{solar} versus R_s and (b) σ_{dc}/σ_{op} for 1D silver nanowires with different diameters d. T_{solar} is the average of TE and TM-polarized incident light. The marker size is proportional to the pitch a of the nanowire array from 10 to 2000 nm. The pitches shown are from 10 to 100 nm in 10 nm increments, 100 to 1000 nm in 100 nm increments and 2000 nm. $a \geq d$.

Finally, we performed simulations of 2D silver nanowire square arrays. We compared T_{solar} averaged for both TE and TM-polarized incident light for 1D silver nanowire arrays with T_{solar} for 2D silver nanowire arrays and found that they agree well with one another. 2D nanowire arrays can be viewed as the two 1D nanowire arrays intersecting one another at 90°, and thus the transmission spectrum of 2D nanowire arrays are approximately the same as that for both TE and TM-incident light averaged together. We also performed finite element analysis to obtain the sheet resistance R_s for 2D silver nanowire arrays, which cannot be derived analytically. The R_s for 2D nanowire arrays are only slightly lower than the 1D nanowire arrays of the same d and a. In Fig. 8, we plot (a) T_{solar} versus R_s for 2D nanowire arrays and (b) σ_{dc}/σ_{op} versus R_s. The plots are approximately the same as that in Fig. 7, though T_{solar} and R_s are both slightly lower.

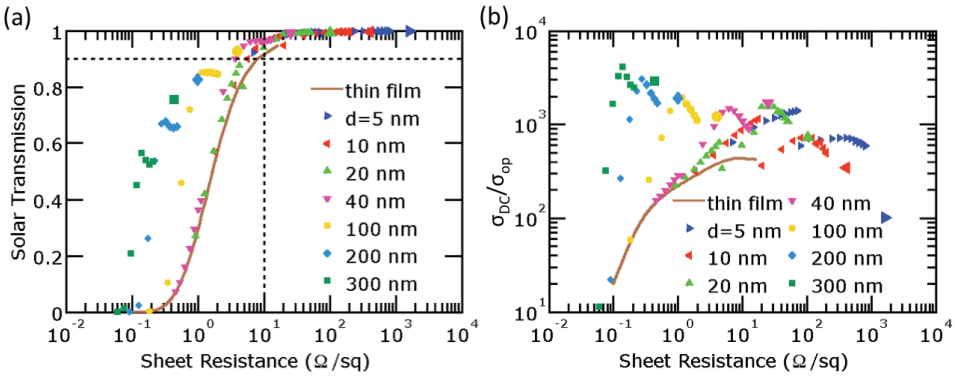

Fig. 8. (a) T_{solar} versus R_s and (b) σ_{dc}/σ_{op} for 2D silver nanowire arrays with different diameters d. The marker size is proportional to the pitch a of the nanowire array from 10 to 2000 nm. The pitches shown are from 10 to 100 nm in 10 nm increments, 100 to 1000 nm in 100 nm increments and 2000 nm. $a \geq d$.

#183390 - $15.00 USD Received 14 Jan 2013; revised 3 Apr 2013; accepted 4 Apr 2013; published 17 Apr 2013

4. Conclusion

Silver thin films and 1D and 2D silver nanowire arrays with a broad range of geometries were investigated as transparent electrodes. The enhanced transmission in silver nanowire arrays is due to indirect propagating modes between the nanowires. For TE-incident light, 1D nanowires have enhanced transmission due to these propagating modes. For TM-incident light, enhanced transmission occurs through direct and indirect propagating modes. When the transmission is primarily through the direct TM_0 mode, there is enhanced transmission, but when both direct and indirect mechanisms are present, asymmetric Fano resonances are observed. These indirect propagating modes are assisted by surface plasmon polaritons. Superior optoelectronic performance was shown for nanowire arrays, which are able to achieve higher T_{solar} for a given R_s. Higher σ_{dc}/σ_{op} may be achieved in nanowire arrays over thin films and higher σ_{dc}/σ_{op} may be achievable in ordered nanowire arrays over current experimental results.

Acknowledgments

The authors would like to thank Professor Irene A. Goldthorpe of the University of Waterloo for helpful discussions. The author P.W.L. would like to acknowledge the support of an Oak Ridge Ralph E. Powe Junior Faculty Enhancement Award.

#183390 - $15.00 USD Received 14 Jan 2013; revised 3 Apr 2013; accepted 4 Apr 2013; published 17 Apr 2013